Analytical Characterization and Production of an Isothermal Surface for Biological and Electronic Applications

Shadi Mahjoob

Kambiz Vafai[1]
e-mail: vafai@engr.ucr.edu

Mechanical Engineering Department,
University of California,
Riverside, CA 92521

Characterization and regulation of isothermal surfaces are key issues in a number of thermal management devices. The surface temperature uniformity can be controlled utilizing a variable area channel heat exchanger filled with a porous medium. A comprehensive analytical investigation of forced convection through a generic variable area channel is carried out to design a compact heat exchanger in producing an isothermal surface subject to a constant heat flux, which may be required in the biological, electronics, optical, laser, manufacturing, and solidification applications. Exact solutions for the fluid and solid phases and the wall surface temperature distributions as well as the Nusselt number correlations are established while incorporating local thermal nonequilibrium and transverse conduction contributions. The channel temperature field is adjusted utilizing either an adiabatic or a constant temperature on the inclined surface. The effects of the pertinent physical parameters, such as channel inlet/outlet thickness, inclination angle, Biot number, ratio of fluid and matrix thermal conductivities, working fluid properties, and imposed heat flux, on the fluid and solid temperature fields and the isothermal surface are thoroughly investigated. The results indicate that utilizing proper pertinent parameters, an isothermal surface is achieved. The validity of the utilization of the local thermal equilibrium model is also investigated and error maps are presented.
[DOI: 10.1115/1.2995690]

Keywords: isothermal surface production, porous media, analytical, PCR

1 Introduction

Porous inserts are quite effective in heat transfer augmentation and thermal control. A porous medium provides an extensive surface area for a given volume between a solid and fluid, which enhances the interstitial heat transfer. As such, porous inserts are an attractive choice for a variety of applications such as solar receiver devices, electronics equipments, building thermal insulation, energy storage units, flat-shaped heat pipes [1,2], catalytic reactors, jet impingement and microchannel cooling technology [3–5], bioheat transfer modeling [6], and recently in biomicrofluidic thermal cyclers [7]. A key issue in a number of heat management devices is the production and regulation of isothermal surfaces by maintaining a relatively constant temperature equal or below a maximum operating temperature for electronic equipment subject to a high heat flux [8,9] such as processors, memory and graphics chips, telecom switches, and high powered military equipments and laser devices, as well as imposing a uniform temperature throughout a biomicrofluidic chip for thermal cycling applications such as polymerase chain reaction (PCR) for nucleic acid (e.g., DNA and RNA) amplification [7,10]. Production of an isothermal surface is also an important issue in thermal therapies (e.g., hyperthermia treatment for cancer tumors [11]), laser light emitting diodes with similar wavelength light, solidification processing [12], single crystal growth [13], turbine blade manufacturing utilizing directional solidification processes [14–17], telescope meniscus mirrors [18], and optical systems [19]. The temperature uniformity can be controlled using a proper utilization of a variable area channel filled with a porous medium. The variation of the channel area can be controlled by the inlet/outlet channel thickness or the angle of the longitudinal direction with respect to the channel upper wall, the so called inclination angle. The velocity and temperature of the working fluid passing through the channel along with its properties (e.g., density, specific heat, and thermal conductivity) are some of the other effective parameters that affect the heat transport augmentation in these types of devices.

Two approaches can be pursued in investigating heat transport through a porous medium utilizing a volume averaging technique: averaging over a representative elementary volume containing both the fluid and the solid phases, and averaging separately over each of the phases, resulting in energy equations for each individual phase [20–24]. These two models are referred to as the one equation model (utilizing local thermal equilibrium assumption) and the two equation model (incorporating the local thermal nonequilibrium condition), respectively [25–29]. The assumption of local thermal equilibrium has been widely used in analyzing transport processes through porous media [28–32]. However, this assumption is not valid for applications where a substantial temperature difference exists between the solid and the fluid phases such as high porosity fibrous materials [25–29,33–35]. Mahjoob and Vafai [33] presented a synthesis of fluid and thermal transport models for metal foams and considered the validity of local thermal equilibrium assumption for foam metal modeling. They also indicated the substantial advantages of utilizing metal foams to improve the performance of heat exchangers considering both heat transfer and pressure drop issues.

Heat transport characteristics in porous media are quite complicated [36–40]. Utilizing the Darcy model and accounting for local thermal nonequilibrium, Lee and Vafai [28] established an exact solution for normalized fluid and solid temperature profiles and the Nusselt number for forced convective flow through a channel filled with a porous medium subject to a constant heat flux. Marafie and Vafai [29] developed an analytical solution utilizing

[1]Corresponding author.

Contributed by the Heat Transfer Division of ASME for publication in the JOURNAL OF HEAT TRANSFER. Manuscript received March 12, 2008; final manuscript received July 9, 2008; published online March 19, 2009. Review conducted by Yogesh Jaluria.

Darcy–Forchheimer–Brinkman model and local thermal nonequilibrium energy transport model and established the temperature profiles and heat transfer correlations. Amiri and Vafai [25,26] employed the generalized model for the momentum equation and local thermal nonequilibrium model for the energy equation, including axial and transverse thermal dispersions to investigate forced convection, and validated their numerical findings utilizing an experimental investigation. They presented detailed error maps for assessing the importance of various simplifying assumptions. Alazmi and Vafai [27] investigated the proper form of boundary conditions for a constant wall heat flux imposed on a porous medium under local thermal nonequilibrium conditions. Effects of variable porosity and thermal dispersion were also analyzed.

In this work, analytical characterizations and production of an isothermal surface for biological (such as in DNA amplification utilizing PCR), electronic, optical, laser, manufacturing, and solidification applications are considered while incorporating the local thermal nonequilibrium conditions. Exact solutions for fluid and solid temperature distributions are presented as well as analytical surface temperature distribution and heat transfer correlations for a generic variable cross sectional area channel filled with a porous medium. Pertinent design parameters affecting the isothermal surface production such as channel inlet/outlet thickness, inclination angle, Biot number, ratio of the fluid and solid thermal conductivities and specific surface area are analytically characterized, and investigated.

2 Modeling and Formulation

2.1 Problem Description. Analysis and design of a highly efficient and compact device for isothermal surface production, when subject to a constant heat flux, are presented in this work. The variable cross sectional area channel heat exchanger is filled with a porous medium, which is attached to a target surface, as shown in Fig. 1. The top part of the channel can be either a constant temperature or an adiabatic surface to minimize losses and control the heat transfer through the channel. The height of the channel inlet is H and the top surface angle relative to the longitudinal direction, the so called inclination angle, is α. Flow is assumed to be hydraulically and thermally fully developed. Natural convection and radiation are assumed to be negligible and all thermodynamic properties of the solid and fluid are considered to be temperature independent. The porous medium is assumed to be homogenous and isotropic.

2.2 Governing Equations. The governing energy equations for the solid and fluid phases incorporating local thermal nonequilibrium conditions are as follows [25,27].

In fluid phase,

$$k_{f,\text{eff}}\nabla_y^2\langle T_f\rangle^f + h_{sf}a_{sf}(\langle T_s\rangle^s - \langle T_f\rangle^f) = \rho c_P\langle u\rangle\frac{\partial\langle T_f\rangle^f}{\partial x} \tag{1}$$

In solid phase,

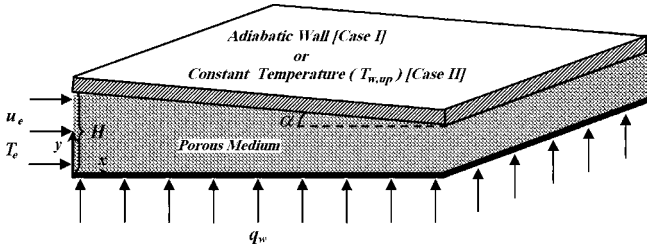

Fig. 1 Schematic of a channel filled with a porous medium subject to a constant heat flux; Case I: adiabatic boundary condition at the upper wall, Case II: constant surface temperature boundary condition at the upper wall

$$k_{s,\text{eff}}\nabla_y^2\langle T_s\rangle^s - h_{sf}a_{sf}(\langle T_s\rangle^s - \langle T_f\rangle^f) = 0 \tag{2}$$

where $k_{f,\text{eff}}$ and $k_{s,\text{eff}}$ are the effective fluid and solid thermal conductivities, ρ is the density, c_p is the specific heat of the fluid, $\langle u\rangle$ is the locally volume averaged fluid velocity, $\langle T_f\rangle^f$ and $\langle T_s\rangle^s$ are the intrinsic phase average fluid and solid temperatures, and h_{sf} and a_{sf} are the interfacial heat transfer coefficient and specific surface area, respectively.

2.3 Boundary Conditions. Based on the work of Amiri et al. [26], Lee and Vafai [28], and Marafie and Vafai [29], the imposed constant heat flux boundary condition under local thermal nonequilibrium conditions can be represented as

$$q_w = -k_{f,\text{eff}}\left.\frac{\partial\langle T_f\rangle^f}{\partial y}\right|_{y=0} - k_{s,\text{eff}}\left.\frac{\partial\langle T_s\rangle^s}{\partial y}\right|_{y=0} \tag{3}$$

In most cases, a solid substrate of finite thickness is attached to the porous medium and the heat flux is applied to the outer wall of the substrate. The heat will then be transferred to the porous medium through the substrate. The temperature at the interface of the porous medium and the solid substrate is likely to be uniform regardless of whether it contacts the solid or fluid. As such, the temperature of the solid and the fluid at the wall interface will be the same [26–28]:

$$\langle T_f\rangle^f|_{y=0} \approx \langle T_s\rangle^s|_{y=0} \approx T_w \tag{4}$$

For the upper wall of the channel, two general thermal boundary conditions are investigated: adiabatic and constant temperature ($T_{w,\text{up}}$) conditions. These are represented as follows.

Case I: Adiabatic boundary condition

$$\left.\frac{\partial\langle T_f\rangle^f}{\partial y}\right|_{y=H-x\tan\alpha} = \left.\frac{\partial\langle T_s\rangle^s}{\partial y}\right|_{y=H-x\tan\alpha} = 0 \tag{5}$$

Case II: Constant wall temperature boundary condition

$$\langle T_f\rangle^f|_{y=H-x\tan\alpha} \approx \langle T_s\rangle^s|_{y=H-x\tan\alpha} \approx T_{w,\text{up}} \tag{6}$$

2.4 Normalization. The governing equations are normalized utilizing the following nondimensional variables:

$$Y = \frac{y}{H - x\tan\alpha}, \quad \psi = \frac{(H - x\tan\alpha)^2}{H^2}, \quad \kappa = \frac{k_{f,\text{eff}}}{k_{s,\text{eff}}},$$
$$\bar{u} = \frac{\langle u\rangle}{u_e H/(H - x\tan\alpha)}, \quad \text{Bi} = \frac{h_{sf}a_{sf}H^2}{k_{s,\text{eff}}} \tag{7}$$

where the parameter ψ is the upper wall shape factor and the parameter κ represents the ratio of fluid to solid thermal conductivities. The parameter Bi is an equivalent Biot number representing the ratio of the conduction resistance within the solid matrix to the thermal resistance associated with the internal convective heat exchange between the matrix and the fluid phase. The temperature is normalized utilizing the above nondimensionalization and considering the two general upper boundary conditions given by the adiabatic and constant wall temperature boundary conditions, respectively, as follows.

Case I: Adiabatic boundary condition

$$\theta = \frac{k_{s,\text{eff}}(\langle T\rangle - T_w)}{Hq_w\sqrt{\psi}} \tag{8}$$

Case II: Constant wall temperature boundary condition

$$\theta = \frac{k_{s,\text{eff}}(\langle T\rangle - T_w)}{Hq_w\sqrt{\psi} + k_{s,\text{eff}}(1+\kappa)(T_{w,\text{up}} - T_w)} \tag{9}$$

Utilizing Eqs. (7)–(9), the governing equations (1) and (2) can be casted as

$$\kappa\frac{\partial^4\theta_f}{\partial Y^4} - (1+\kappa)\text{Bi}\cdot\psi\left(\frac{\partial^2\theta_f}{\partial Y^2}\right) = -\text{Bi}\cdot\psi \tag{10}$$

$$\kappa\frac{\partial^4\theta_s}{\partial Y^4}-(1+\kappa)\mathrm{Bi}\cdot\psi\left(\frac{\partial^2\theta_s}{\partial Y^2}\right)=-\mathrm{Bi}\cdot\psi \tag{11}$$

along with the following boundary conditions for the lower boundary:

$$\theta_f|_{Y=0}=\theta_s|_{Y=0}=0 \tag{12}$$

and the upper boundary as follows.

Case I: Adiabatic boundary condition

$$\left.\frac{\partial\theta_f}{\partial Y}\right|_{Y=1}=\left.\frac{\partial\theta_s}{\partial Y}\right|_{Y=1}=0 \tag{13}$$

Case II: Constant wall temperature boundary condition

$$\theta_f|_{Y=1}=\theta_s|_{Y=1}=\theta_{w,\mathrm{up}} \tag{14}$$

where

$$\theta_{w,\mathrm{up}}=\frac{k_{s,\mathrm{eff}}(T_{w,\mathrm{up}}-T_w)}{Hq_w\sqrt{\psi}+k_{s,\mathrm{eff}}(1+\kappa)(T_{w,\mathrm{up}}-T_w)} \tag{15}$$

Additional boundary conditions can be obtained by evaluating the second derivatives of θ_f and θ_s at the wall, which results in

$$\left.\frac{\partial^2\theta_f}{\partial Y^2}\right|_{Y=0}=1/\kappa,\qquad\left.\frac{\partial^2\theta_s}{\partial Y^2}\right|_{Y=0}=0 \tag{16}$$

A set of extra boundary conditions is obtained utilizing the governing equations and evaluating them at $Y=1$ along with Eq. (13) or (14) for the upper boundary for adiabatic and constant wall temperature cases, respectively. This results in the fourth set of required boundary conditions given by the following.

Case I: Adiabatic boundary condition

$$\left.\frac{\partial^3\theta_f}{\partial Y^3}\right|_{Y=1}=\left.\frac{\partial^3\theta_s}{\partial Y^3}\right|_{Y=1}=0 \tag{17}$$

Case II: Constant wall temperature boundary condition

$$\left.\frac{\partial^2\theta_f}{\partial Y^2}\right|_{Y=1}=1/\kappa,\qquad\left.\frac{\partial^2\theta_s}{\partial Y^2}\right|_{Y=1}=0 \tag{18}$$

2.5 Fluid, Solid, and Wall Temperature Fields. The fluid and solid phase temperature distributions can be obtained by solving the governing equations and boundary conditions given by Eqs. (10)–(12) and (16), and additional boundary conditions given by Eqs. (13) and (17) for an adiabatic and Eqs. (14) and (18) for a constant temperature upper wall boundary, respectively. Differential equations (10) and (11) are solved and modified using the appropriate Neumann and Dirichlet boundary conditions obtained earlier. After considerable analysis, this results in the following results for fluid, solid, fluid bulk-mean, and wall temperature profiles.

Case I: Adiabatic boundary condition

$$\theta_f=\frac{1}{1+\kappa}\left(Y\left(\frac{Y}{2}-1\right)-\frac{1}{(1+\kappa)\mathrm{Bi}\psi}\left\{1-\frac{e^{\lambda Y}+e^{\lambda(2-Y)}}{1+e^{2\lambda}}\right\}\right) \tag{19}$$

$$\theta_s=\frac{1}{1+\kappa}\left(Y\left(\frac{Y}{2}-1\right)+\frac{\kappa}{(1+\kappa)\mathrm{Bi}\psi}\left\{1-\frac{e^{\lambda Y}+e^{\lambda(2-Y)}}{1+e^{2\lambda}}\right\}\right) \tag{20}$$

where

$$\lambda=\sqrt{\mathrm{Bi}\psi(1+\kappa)/\kappa} \tag{21}$$

and

$$\Delta\theta=\theta_s-\theta_f=\frac{1}{(1+\kappa)\mathrm{Bi}\psi}\left(1-\frac{e^{\lambda Y}+e^{\lambda(2-Y)}}{1+e^{2\lambda}}\right) \tag{22}$$

$$\theta_{f,b}=\frac{-1}{1+\kappa}\left(\frac{1}{3}+\frac{1}{(1+\kappa)\mathrm{Bi}\psi}\left\{1-\frac{1}{\lambda}\frac{e^{2\lambda}-1}{e^{2\lambda}+1}\right\}\right) \tag{23}$$

$$T_w=\frac{q_w}{\rho c_p H u_e}x+T_e+\frac{q_w(H-x\tan\alpha)}{k_{s,\mathrm{eff}}(1+\kappa)}\left(\frac{1}{3}+\frac{1}{(1+\kappa)\mathrm{Bi}\psi}\times\left\{1-\frac{1}{\lambda}\frac{e^{2\lambda}-1}{e^{2\lambda}+1}\right\}\right) \tag{24}$$

Case II: Constant wall temperature boundary condition

$$\theta_f=\frac{1}{1+\kappa}\left(Y\left(\frac{Y}{2}+(1+\kappa)\theta_{w,\mathrm{up}}-\frac{1}{2}\right)-\frac{1}{(1+\kappa)\mathrm{Bi}\psi}\left\{1-\frac{e^{\lambda Y}+e^{\lambda(1-Y)}}{1+e^{\lambda}}\right\}\right) \tag{25}$$

$$\theta_s=\frac{1}{1+\kappa}\left(Y\left(\frac{Y}{2}+(1+\kappa)\theta_{w,\mathrm{up}}-\frac{1}{2}\right)+\frac{\kappa}{(1+\kappa)\mathrm{Bi}\psi}\left\{1-\frac{e^{\lambda Y}+e^{\lambda(1-Y)}}{1+e^{\lambda}}\right\}\right) \tag{26}$$

where

$$\lambda=\sqrt{\mathrm{Bi}\psi(1+\kappa)/\kappa}$$

and

$$\Delta\theta=\theta_s-\theta_f=\frac{1}{(1+\kappa)\mathrm{Bi}\psi}\left(1-\frac{e^{\lambda Y}+e^{\lambda(1-Y)}}{1+e^{\lambda}}\right) \tag{27}$$

$$\theta_{f,b}=\frac{-1}{1+\kappa}\left(\frac{1}{12}-\frac{(1+\kappa)\theta_{w,\mathrm{up}}}{2}+\frac{1}{(1+\kappa)\mathrm{Bi}\psi}\left\{1-\frac{2}{\lambda}\frac{e^{\lambda}-1}{e^{\lambda}+1}\right\}\right) \tag{28}$$

$$T_{f,b}=\left(T_e-T_{w,\mathrm{up}}-\frac{q_wH}{2k_{s,\mathrm{eff}}(1+\kappa)}\right)\exp\left[\frac{-12\mathrm{Bi}k_{s,\mathrm{eff}}(1+\kappa)^2x}{\rho c_p u_e H^2\left(7\mathrm{Bi}(1+\kappa)+12\left(1-\frac{2(e^{\lambda}-1)}{\lambda(e^{\lambda}+1)}\right)\right)}\right]+T_{w,\mathrm{up}}+\frac{q_wH}{2k_{s,\mathrm{eff}}(1+\kappa)}\quad\text{for }\alpha=0 \tag{29a}$$

$$T_{f,b}=\frac{1}{2}(T_w+T_{w,\mathrm{up}})+\left[\frac{1}{12}+\frac{1}{\mathrm{Bi}\psi(1+\kappa)}\left(1-\frac{2(e^{\lambda}-1)}{\lambda(e^{\lambda}+1)}\right)\right]\left(T_w-T_{w,\mathrm{up}}-\frac{q_w(H-x\tan(\alpha))}{k_{s,\mathrm{eff}}(1+\kappa)}\right)\quad\text{for }\alpha\neq0 \tag{29b}$$

$$T_w(x)=\left(T_{w,x=0}-T_{w,\mathrm{up}}-\frac{q_wH}{k_{s,\mathrm{eff}}(1+\kappa)}\right)\exp\left[\frac{-12\mathrm{Bi}k_{s,\mathrm{eff}}(1+\kappa)^2x}{\rho c_p u_e H^2\left(7\mathrm{Bi}(1+\kappa)+12\left(1-\frac{2(e^{\lambda}-1)}{\lambda(e^{\lambda}+1)}\right)\right)}\right]+\frac{q_wH}{k_{s,\mathrm{eff}}(1+\kappa)}+T_{w,\mathrm{up}}\quad\text{for }\alpha=0 \tag{30a}$$

$$T_w(x) = \exp\left(-\int_0^x A(\xi)d\xi\right)\left[\int_0^x \exp\left(\int_0^\xi A(\xi)d\xi\right)B(\xi)d\xi + T_{w,x=0}\right] \quad \text{for } \alpha \neq 0 \tag{30b}$$

where

$$A(\xi) = \frac{\dfrac{k_{s,\text{eff}}(1+\kappa)}{\rho c_p u_e H^2 \psi_1^{1/2}} + \dfrac{2\tan(\alpha)}{H\text{Bi}(1+\kappa)\psi_1^{3/2}}\left(\dfrac{(\lambda_1-3)e^{2\lambda_1}+4\lambda_1 e^{\lambda_1}+\lambda_1+3}{\lambda_1(e^{\lambda_1}+1)^2}\right)}{\dfrac{7}{12}+\dfrac{1}{\text{Bi}\psi_1(1+\kappa)}\left(1-\dfrac{2(e^{\lambda_1}-1)}{\lambda_1(e^{\lambda_1}+1)}\right)} \tag{30c}$$

$$B(\xi) = \frac{\left\{\begin{array}{l}\left[\dfrac{k_{s,\text{eff}}(1+\kappa)}{\rho c_p u_e H^2 \psi_1^{1/2}} + \dfrac{2\tan(\alpha)}{H\text{Bi}(1+\kappa)\psi_1^{3/2}}\left(\dfrac{(\lambda_1-3)e^{2\lambda_1}+4\lambda_1 e^{\lambda_1}+\lambda_1+3}{\lambda_1(e^{\lambda_1}+1)^2}\right)\right]T_{w,\text{up}} \\ +\dfrac{q_w\tan(\alpha)}{k_{s,\text{eff}}(1+\kappa)^2\text{Bi}\psi_1}\left[\dfrac{-(1+\kappa)\text{Bi}\psi_1}{12}+\dfrac{2(e^{\lambda_1}(\lambda_1+1)-1)}{\lambda_1(e^{\lambda_1}+1)}+\dfrac{2(-3(e^{\lambda_1}+1)-\lambda_1 e^{\lambda_1})(e^{\lambda_1}-1)}{\lambda_1(e^{\lambda_1}+1)^2}+1\right]+\dfrac{q_w}{\rho c_p u_e H}\end{array}\right\}}{\dfrac{7}{12}+\dfrac{1}{\text{Bi}\psi_1(1+\kappa)}\left(1-\dfrac{2(e^{\lambda_1}-1)}{\lambda_1(e^{\lambda_1}+1)}\right)} \tag{30d}$$

$$\psi_1 = \frac{(H-\xi\tan\alpha)^2}{H^2} \tag{30e}$$

$$\lambda_1 = \frac{\sqrt{\text{Bi}(1+\kappa)/\kappa}}{H}(H-\xi\tan\alpha) \tag{30f}$$

and

$$T_{w,x=0} = \frac{\dfrac{q_w H + k_{s,\text{eff}}(1+\kappa)T_{w,\text{up}}}{k_{s,\text{eff}}\text{Bi}(1+\kappa)^2}\left(1-\dfrac{2(e^{\Delta}-1)}{\Delta(e^{\Delta}+1)}\right)+\dfrac{q_w H}{12k_{s,\text{eff}}(1+\kappa)}-\dfrac{5}{12}T_{w,\text{up}}+T_e}{\dfrac{7}{12}+\dfrac{1}{\text{Bi}(1+\kappa)}\left(1-\dfrac{2(e^{\Delta}-1)}{\Delta(e^{\Delta}+1)}\right)} \tag{31}$$

where

$$\Delta = \sqrt{\text{Bi}(1+\kappa)/\kappa} \tag{32}$$

A simplified solution for the wall and fluid bulk-mean temperature distributions at nonzero inclination angle for Case II can be obtained when $x\tan\alpha$ is significantly smaller than the inlet of the channel.

$$T_w(x) = \Lambda + (T_{w,x=0}-\Lambda)\exp\left[\frac{-12\text{Bi}\psi k_{s,\text{eff}}(1+\kappa)^2 - 24\rho c_p u_e H\tan(\alpha)\left(\dfrac{(\lambda-3)e^{2\lambda}+4\lambda e^{\lambda}+\lambda+3}{\lambda(e^{\lambda}+1)^2}\right)}{\rho c_p u_e H^2\left\{7\text{Bi}\psi^{3/2}(1+\kappa)+12\psi^{1/2}\left(1-\dfrac{2(e^{\lambda}-1)}{\lambda(e^{\lambda}+1)}\right)\right\}}x\right] \quad \text{for } \alpha \neq 0 \tag{33}$$

$$\begin{aligned} T_{f,b} = {} & \left[\frac{7}{12}+\frac{1}{\text{Bi}\psi(1+\kappa)}\left(1-\frac{2(e^{\lambda}-1)}{\lambda(e^{\lambda}+1)}\right)\right] \\ & \times\left\{\Lambda+(T_{w,x=0}-\Lambda)\exp\left[\frac{-12\text{Bi}\psi k_{s,\text{eff}}(1+\kappa)^2-24\rho c_p u_e H\tan(\alpha)\left(\dfrac{(\lambda-3)e^{2\lambda}+4\lambda e^{\lambda}+\lambda+3}{\lambda(e^{\lambda}+1)^2}\right)}{\rho c_p u_e H^2\left\{7\text{Bi}\psi^{3/2}(1+\kappa)+12\psi^{1/2}\left(1-\dfrac{2(e^{\lambda}-1)}{\lambda(e^{\lambda}+1)}\right)\right\}}x\right]\right\} \\ & +\frac{T_{w,\text{up}}}{2}-\left[\frac{1}{12}+\frac{1}{\text{Bi}\psi(1+\kappa)}\left(1-\frac{2(e^{\lambda}-1)}{\lambda(e^{\lambda}+1)}\right)\right]\left(T_{w,\text{up}}+\frac{q_w(H-x\tan(\alpha))}{k_{s,\text{eff}}(1+\kappa)}\right) \quad \text{for } \alpha \neq 0 \end{aligned} \tag{34}$$

where

$$\Lambda = T_{w,\mathrm{up}} + \frac{\rho c_p u_e H^2 q_w \tan(\alpha)\psi^{1/2}\left[-\frac{(1+\kappa)\mathrm{Bi}\psi}{12} + \frac{2(e^{\lambda}(\lambda+1)-1)}{\lambda(e^{\lambda}+1)} + \frac{2(-3(e^{\lambda}+1)-\lambda e^{\lambda})(e^{\lambda}-1)}{\lambda(e^{\lambda}+1)^2} + 1\right] + q_w H k_{s,\mathrm{eff}}(1+\kappa)^2\mathrm{Bi}\psi^{3/2}}{k_{s,\mathrm{eff}}(1+\kappa)\left\{k_{s,\mathrm{eff}}(1+\kappa)^2\mathrm{Bi}\psi + 2H\rho c_p u_e \tan(\alpha)\left(\frac{(\lambda-3)e^{2\lambda}+4\lambda e^{\lambda}+\lambda+3}{\lambda(e^{\lambda}+1)^2}\right)\right\}} \tag{35}$$

2.6 Heat Transfer Correlations. The wall heat transfer coefficient for the local thermal nonequilibrium model is obtained from

$$h_{w,\mathrm{nonequil}} = \frac{q_w}{T_w - T_{f,b}} \tag{36}$$

Case I: Adiabatic boundary condition

The Nusselt number at the channel wall subject to a constant heat flux can be represented as

$$\mathrm{Nu}_{w,\mathrm{nonequil}} = \frac{h_{w,\mathrm{nonequil}} D_h}{k_{f,\mathrm{eff}}} = \frac{-2}{\kappa\sqrt{\psi}\theta_{f,b}} \tag{37}$$

Utilizing Eq. (23) and after some manipulation,

$$\mathrm{Nu}_{w,\mathrm{nonequil}} = 6\frac{1+\kappa}{\kappa\sqrt{\psi}}\frac{1}{1+\frac{3}{(1+\kappa)\mathrm{Bi}\psi}\left(1-\frac{1}{\lambda}\frac{e^{2\lambda}-1}{e^{2\lambda}+1}\right)} \tag{38}$$

Case II: Constant wall temperature boundary condition

Using Eq. (9), the Nusselt number at the channel wall subject to a constant heat flux can be represented as

$$\mathrm{Nu}_{w,\mathrm{nonequil}} = \frac{h_{w,\mathrm{nonequil}} D_h}{k_{f,\mathrm{eff}}} = \frac{-2}{\kappa\theta_{f,b}\left(\sqrt{\psi} + \frac{k_{s,\mathrm{eff}}(1+\kappa)}{q_w H}(T_{w,\mathrm{up}} - T_w)\right)} \tag{39}$$

Utilizing Eq. (28) and after some manipulation, the Nusselt number can be represented as

$$\mathrm{Nu}_{w,\mathrm{nonequil}} = \frac{24\frac{1+\kappa}{\kappa}}{6+\left\{-5+\frac{12\left(1-\frac{2}{\lambda}\frac{e^{\lambda}-1}{e^{\lambda}+1}\right)}{(1+\kappa)\mathrm{Bi}}\right\}\times\left[\frac{k_{s,\mathrm{eff}}(1+\kappa)}{q_w H}(T_{w,\mathrm{up}} - T_{w,x=0}) + 1\right]\exp\left[\frac{-12\mathrm{Bi}k_{s,\mathrm{eff}}(1+\kappa)^2 x}{\rho c_p u_e H^2\left(7\mathrm{Bi}(1+\kappa) + 12\left(1-\frac{2(e^{\lambda}-1)}{\lambda(e^{\lambda}+1)}\right)\right)}\right]} \quad \text{for } \alpha = 0 \tag{40a}$$

$$\mathrm{Nu}_{w,\mathrm{nonequil}} = \frac{24\frac{1+\kappa}{\kappa\sqrt{\psi}}}{1+\frac{12}{\mathrm{Bi}\psi(1+\kappa)}\left(1-\frac{2}{\lambda}\frac{e^{\lambda}-1}{e^{\lambda}+1}\right)+\frac{k_{s,\mathrm{eff}}(1+\kappa)}{q_w H\sqrt{\psi}}(T_{w,\mathrm{up}} - T_w)\left\{-5+\frac{12}{\mathrm{Bi}\psi(1+\kappa)}\left(1-\frac{2}{\lambda}\frac{e^{\lambda}-1}{e^{\lambda}+1}\right)\right\}} \quad \text{for } \alpha \neq 0 \tag{40b}$$

2.7 Local Thermal Equilibrium Model. The energy equation for the one equation model can be obtained by adding Eqs. (1) and (2) assuming thermal equilibrium between the fluid and solid phases with the following boundary conditions:

$$\theta|_{Y=0} = 0 \tag{41}$$

and

$$\left.\frac{\partial\theta}{\partial Y}\right|_{Y=1} = 0 \quad \text{for Case I: Adiabatic boundary condition} \tag{42}$$

$$\theta|_{Y=1} = \theta_{w,\mathrm{up}} \quad \text{for Case II: Constant wall temperature boundary condition} \tag{43}$$

where $\theta_{w,\mathrm{up}}$ is defined in Eq. (15).

Based on the local thermal equilibrium model, the following results for the wall, the temperature field, and the Nusselt number are obtained.

Case I: Adiabatic boundary condition

$$\theta = \frac{Y}{1+\kappa}\left(\frac{Y}{2} - 1\right) \tag{44}$$

$$T_w = \left(\frac{1}{\rho c_p H u_e} - \frac{\tan(\alpha)}{3(k_{f,\mathrm{eff}} + k_{s,\mathrm{eff}})}\right)q_w x + T_e + \frac{q_w H}{3(k_{f,\mathrm{eff}} + k_{s,\mathrm{eff}})} \tag{45}$$

$$\mathrm{Nu}_{w,\mathrm{equil}} = 6[(1+\kappa)/\kappa\sqrt{\psi}] \tag{46}$$

Case II: Constant wall temperature boundary condition

$$\theta = \frac{Y}{1+\kappa}\left(\frac{Y}{2} + (1+\kappa)\theta_{w,\mathrm{up}} - \frac{1}{2}\right) \tag{47}$$

$$T_w(x) = \left(T_{w,x=0} - T_{w,\mathrm{up}} - \frac{q_w H}{k_{s,\mathrm{eff}}(1+\kappa)}\right)\exp\left[\frac{-12k_{s,\mathrm{eff}}(1+\kappa)x}{7\rho c_p u_e H^2}\right] + \frac{q_w H}{k_{s,\mathrm{eff}}(1+\kappa)} + T_{w,\mathrm{up}} \quad \text{for } \alpha = 0 \tag{48a}$$

$$T_w(x) = T_{w,\mathrm{up}} + \frac{q_w(H - x\tan(\alpha))}{1 - \dfrac{12k_{s,\mathrm{eff}}(1+\kappa)}{7\rho c_p u_e H\tan(\alpha)}}\left(\frac{1}{7k_{s,\mathrm{eff}}(1+\kappa)} - \frac{12}{7\rho c_p u_e H\tan(\alpha)}\right) + \left[T_{w,x=0} - T_{w,\mathrm{up}} - \frac{q_w H}{1 - \dfrac{12k_{s,\mathrm{eff}}(1+\kappa)}{7\rho c_p u_e H\tan(\alpha)}}\left(\frac{1}{7k_{s,\mathrm{eff}}(1+\kappa)} - \frac{12}{7\rho c_p u_e H\tan(\alpha)}\right)\right]\left(\frac{H - x\tan(\alpha)}{H}\right)^{12k_{s,\mathrm{eff}}(1+\kappa)/7\rho c_p u_e H\tan(\alpha)} \quad \text{for } \alpha \neq 0 \tag{48b}$$

$$\mathrm{Nu}_{w,\mathrm{equil}} = \frac{24\dfrac{1+\kappa}{\kappa}}{6 - 5\left(\dfrac{k_{s,\mathrm{eff}}(1+\kappa)}{q_w H}(T_{w,\mathrm{up}} - T_{w,x=0}) + 1\right)\exp\left[\dfrac{-12k_{s,\mathrm{eff}}(1+\kappa)x}{7\rho c_p u_e H^2}\right]} \quad \text{for } \alpha = 0 \tag{49a}$$

$$\mathrm{Nu}_{w,\mathrm{equil.}} = \frac{24\dfrac{1+\kappa}{\kappa\sqrt{\psi}}}{1 + \dfrac{5k_{s,\mathrm{eff}}(1+\kappa)}{1 - \dfrac{12k_{s,\mathrm{eff}}(1+\kappa)}{7\rho c_p u_e H\tan(\alpha)}}\left[\dfrac{1}{7k_{s,\mathrm{eff}}(1+\kappa)} - \dfrac{12}{7\rho c_p u_e H\tan(\alpha)}\right] - 5\times\left[\dfrac{k_{s,\mathrm{eff}}(1+\kappa)}{q_w H}\left(T_{w,up} - T_{w,x=0}\right) + \dfrac{k_{s,\mathrm{eff}}(1+\kappa)}{\left(1 - \dfrac{12k_{s,\mathrm{eff}}(1+\kappa)}{7\rho c_p u_e H\tan(\alpha)}\right)}\times\left(\dfrac{1}{7k_{s,\mathrm{eff}}(1+\kappa)} - \dfrac{12}{7\rho c_p u_e H\tan(\alpha)}\right)\right]\times\psi^{\left(\frac{6k_{s,\mathrm{eff}}(1+\kappa)}{7\rho c_p u_e H\tan(\alpha)} - \frac{1}{2}\right)}} \quad \text{for } \alpha \neq 0 \tag{49b}$$

where

$$T_{w,x=0} = \frac{q_w H}{7k_{s,\mathrm{eff}}(1+\kappa)} - \frac{5}{7}T_{w,\mathrm{up}} + \frac{12}{7}T_e \tag{50}$$

The error in utilization of the local thermal equilibrium is established based on Nusselt number expressions derived for the local thermal equilibrium and nonequilibrium models:

$$E = \frac{\mathrm{Nu}_{w,\mathrm{equil}} - \mathrm{Nu}_{w,\mathrm{nonequil}}}{\mathrm{Nu}_{w,\mathrm{nonequil}}} \tag{51}$$

This results in the following expressions.

Case I: Adiabatic boundary condition

$$E = \frac{3}{(1+\kappa)\mathrm{Bi}\psi}\left[1 - \frac{1}{\lambda}\frac{e^{2\lambda} - 1}{e^{2\lambda} + 1}\right] \tag{52}$$

Case II: Constant wall temperature boundary condition

$$E = \frac{\left\{6 + \left\{-5 + \dfrac{12\left(1 - \dfrac{2}{\lambda}\dfrac{e^{\lambda} - 1}{e^{\lambda} + 1}\right)}{(1+\kappa)\mathrm{Bi}}\right\}\times\left[\dfrac{k_{s,\mathrm{eff}}(1+\kappa)}{q_w H}(T_{w,\mathrm{up}} - T_{w,x=0}) + 1\right]\exp\left[\dfrac{-12\mathrm{Bi}k_{s,\mathrm{eff}}(1+\kappa)^2 x}{\rho c_p u_e H^2\left(7\mathrm{Bi}(1+\kappa) + 12\left(1 - \dfrac{2(e^{\lambda} - 1)}{\lambda(e^{\lambda} + 1)}\right)\right)}\right]}{6 - 5\left(\dfrac{k_{s,\mathrm{eff}}(1+\kappa)}{q_w H}(T_{w,\mathrm{up}} - T_{w,x=0}) + 1\right)\exp\left[\dfrac{-12k_{s,\mathrm{eff}}(1+\kappa)}{7\rho c_p u_e H^2}x\right]} - 1 \quad \text{for } \alpha = 0 \tag{53a}$$

$$E = \frac{1+\dfrac{12}{Bi\psi(1+\kappa)}\left(1-\dfrac{2}{\lambda}\dfrac{e^{\lambda}-1}{e^{\lambda}+1}\right)+\dfrac{k_{s,\mathrm{eff}}(1+\kappa)}{q_w H\sqrt{\psi}}\left(T_{w,\mathrm{up}}-T_w\right)\left\{-5+\dfrac{12}{Bi\psi(1+\kappa)}\left(1-\dfrac{2}{\lambda}\dfrac{e^{\lambda}-1}{e^{\lambda}+1}\right)\right\}}{1+\dfrac{5k_{s,\mathrm{eff}}(1+\kappa)}{1-\dfrac{12k_{s,\mathrm{eff}}(1+\kappa)}{7\rho c_p u_e H\tan(\alpha)}}\left[\dfrac{\dfrac{1}{7k_{s,\mathrm{eff}}(1+\kappa)}-}{\dfrac{12}{7\rho c_p u_e H\tan(\alpha)}}\right]-5\left[\begin{array}{l}\dfrac{k_{s,\mathrm{eff}}(1+\kappa)}{q_w H}\left(T_{w,\mathrm{up}}-T_{w,x=0}\right)+\\ \dfrac{k_{s,\mathrm{eff}}(1+\kappa)}{\left(1-\dfrac{12k_{s,\mathrm{eff}}(1+\kappa)}{7\rho c_p u_e H\tan(\alpha)}\right)}\times\\ \left(\dfrac{1}{7k_{s,\mathrm{eff}}(1+\kappa)}-\dfrac{12}{7\rho c_p u_e H\tan(\alpha)}\right)\end{array}\right]\times\psi^{\left(\frac{6k_{s,\mathrm{eff}}(1+\kappa)}{7\rho c_p u_e H\tan(\alpha)}-\frac{1}{2}\right)}}-1$$

$$\text{for } \alpha \neq 0 \tag{53b}$$

3 Results and Discussion

The effect of pertinent parameters and their physical effects on fluid and solid phase temperature distributions and heat transfer are quite important in characterizing the production of an isothermal surface. The analytical temperature profiles are compared with the numerical results at different inclination angles and longitudinal locations, and also with the exact solutions by Lee and Vafai [28] and Marafie and Vafai [29] for a rectangular channel. In these studies [28,29], forced convection flow through a channel filled with a porous medium was investigated in which the upper and lower channel walls were subjected to a constant heat flux. Due to the symmetric geometry in these works [28,29], the channel centerline can be modeled as an adiabatic wall. As such, the

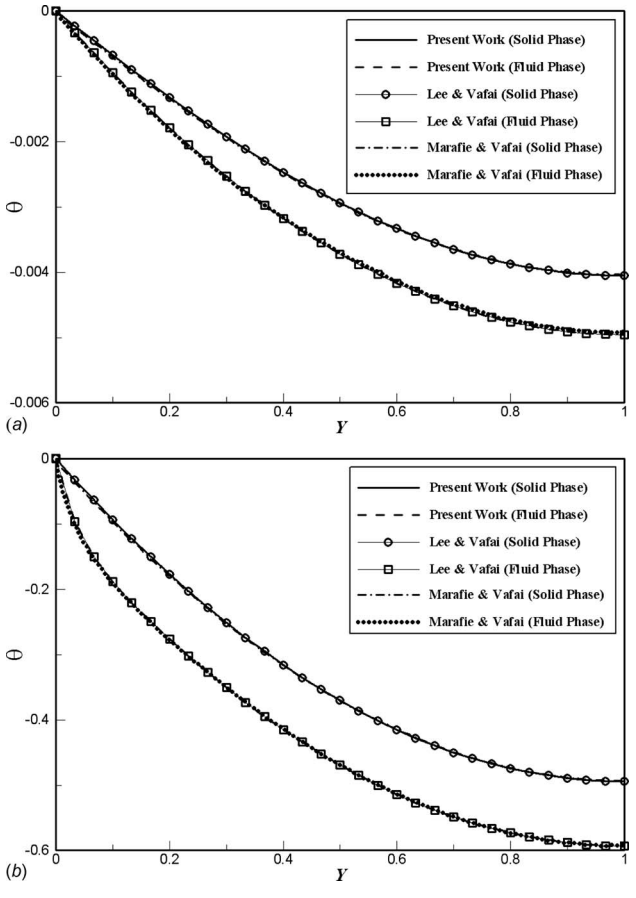

Fig. 2 Comparison of the present analytical temperature distributions for fluid and solid phases with analytical solutions by Lee and Vafai [28] and Marafie and Vafai [29] at α=0 deg and Bi=10. (*a*) κ=100 and (*b*) κ=0.01.

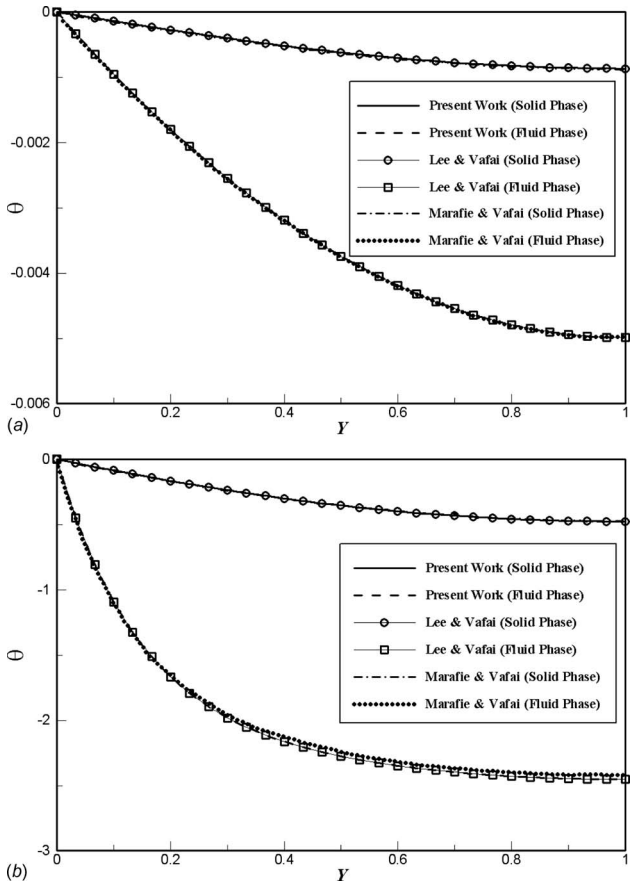

Fig. 3 Comparison of the present analytical temperature distributions for fluid and solid phases with analytical solutions by Lee and Vafai [28] and Marafie and Vafai [29] at α=0 deg and Bi=0.5. (*a*) κ=100 and (*b*) κ=0.01.

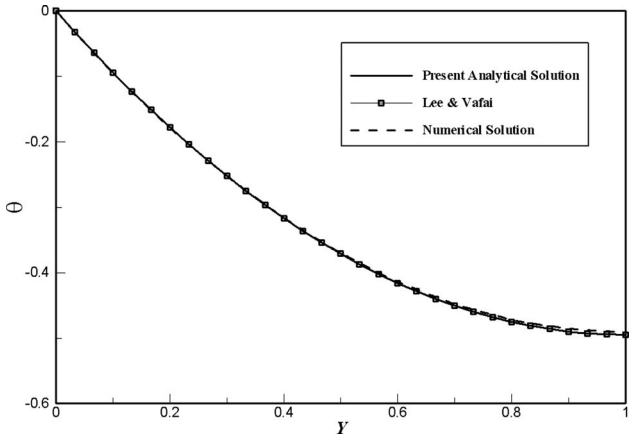

Fig. 4 Comparison of the temperature distribution for the one equation model obtained from the present analytical work, with the analytical solution of Lee and Vafai [28] and computational simulation for $\kappa=5\times10^{-5}$ and $\alpha=0$ deg

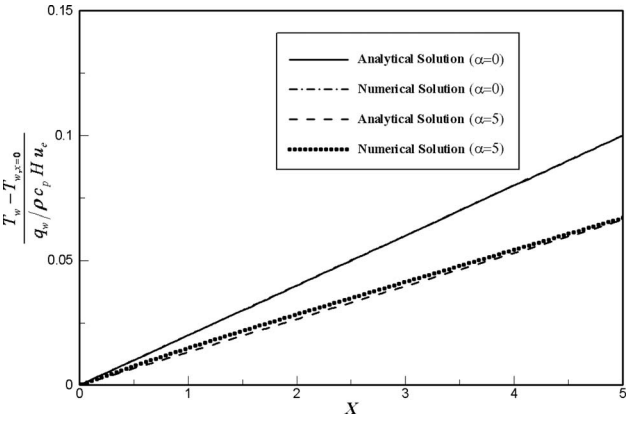

Fig. 6 Comparison between the wall temperature profile obtained from the present analytical solution and numerical simulation utilizing one equation model, at the inclination angles of 0 deg and 5 deg

results from Refs. [28,29] can be compared with the present exact solutions for zero inclination angle when an adiabatic boundary condition is employed for the upper wall of the channel. For numerical simulations, an implicit, pressure-based, cell-centered finite volume method is utilized to solve the coupled nonlinear governing equations. The governing equations including Darcy–Forchheimer–Brinkman momentum equation and the energy equation with local thermal equilibrium assumption are discretized and linearized, utilizing second order upwind method for the convection terms and central differencing for the diffusion terms. Resulting algebraic equations are solved sequentially using Gauss–Seidel point implicit linear equation solver in conjunction with an algebraic multigrid (AMG) method in order to reduce the dispersion errors while increasing the computational speed [41]. As such, first, the momentum equations are solved to obtain the velocity field. Next, the continuity equation is solved utilizing the SIMPLE algorithm for the pressure-velocity coupling to obtain and

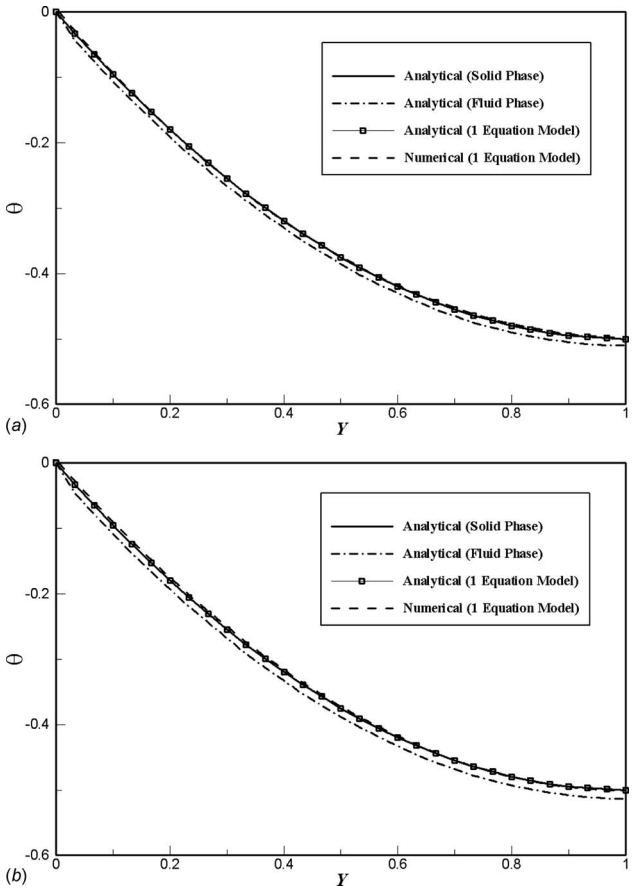

Fig. 5 Comparison of the present analytical temperature distributions (utilizing the exact solutions of two and one equation models) with the numerical simulations at $\alpha=2$ deg, Bi=100, and $\kappa=5\times10^{-5}$. (*a*) $X=1$ and (*b*) $X=4$.

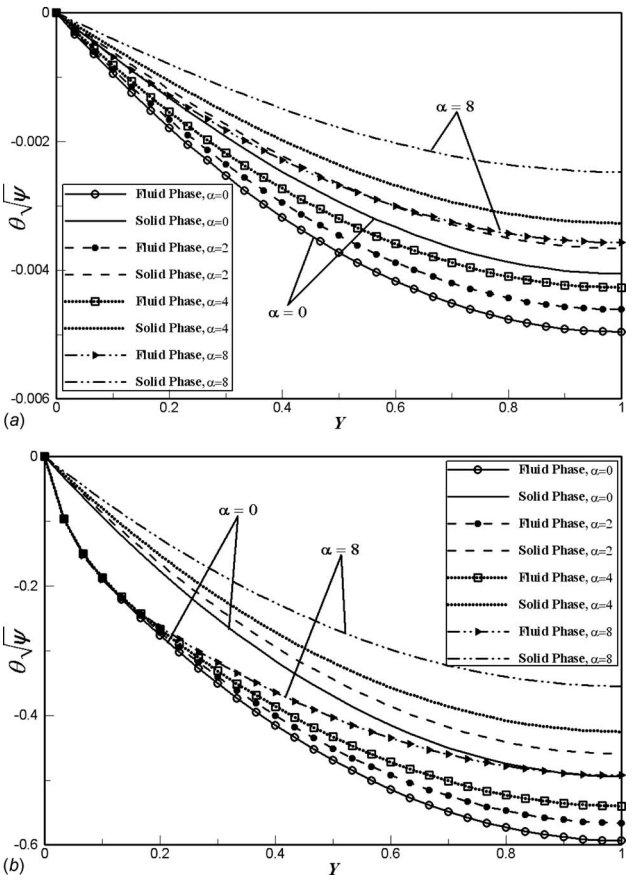

Fig. 7 Effect of inclination angle on fluid and solid temperature fields for Bi=10 at $X=2$. (*a*) $\kappa=100$ and (*b*) $\kappa=0.01$.

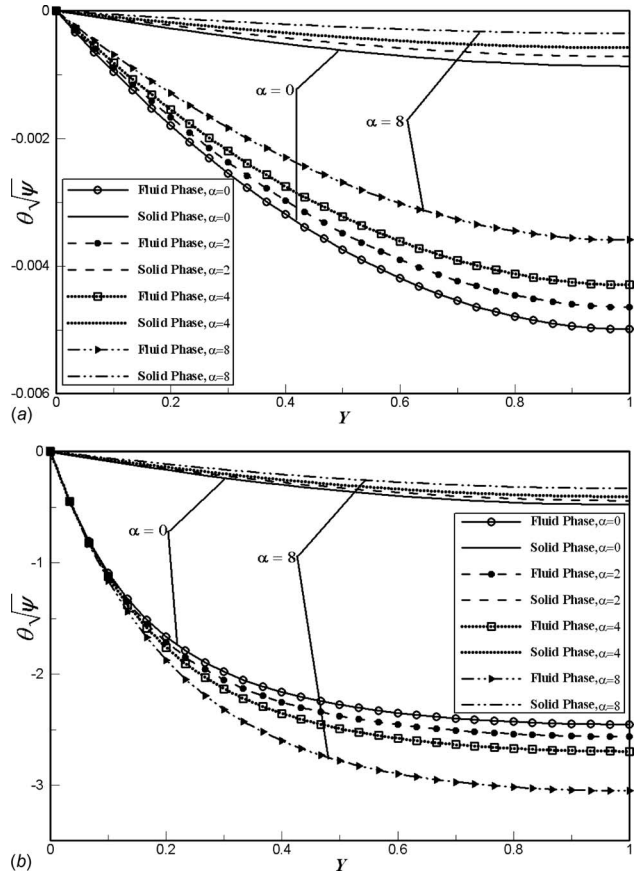

Fig. 8 Effect of inclination angle on fluid and solid temperature fields for Bi=0.5 at $X=2$. (*a*) $\kappa=100$ and (*b*) $\kappa=0.01$.

modify the pressure field, mass fluxes, and the velocity field [42]. Finally, the energy equation is solved to obtain the temperature field. An iterative procedure utilizing under-relaxation is used. Convergence is assumed when residuals become less than 10^{-6}.

Fluid and solid phase temperature distributions at zero inclination angle were found to be in excellent agreement with the analytical results by Lee and Vafai [28] and Marafie and Vafai [29]. The temperature profiles are compared with four sets of Biot numbers (Bi) and ratios of effective fluid to solid thermal conductivities (κ), as shown in Figs. 2 and 3. The small deviation in the

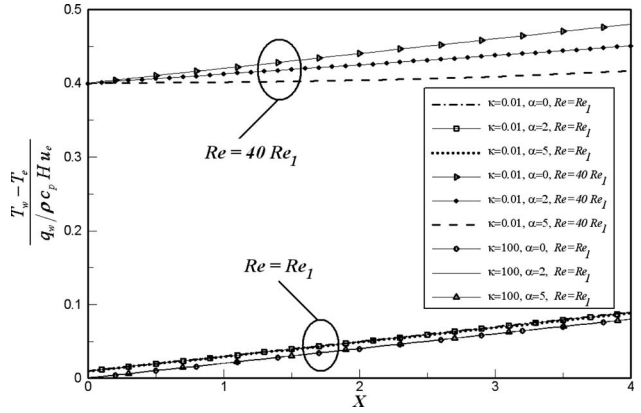

Fig. 9 Effect of the inclination angle (α), flow rate, and effective thermal conductivity ratio (κ) on the normalized wall temperature distribution for Bi=10

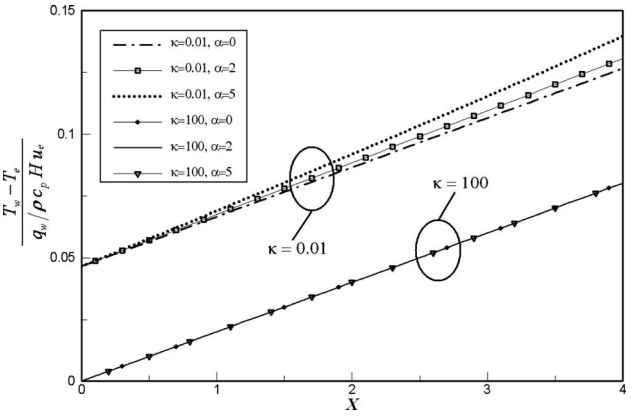

Fig. 10 Effect of the inclination angle (α) and effective thermal conductivity ratio (κ) on the normalized wall temperature distribution for Bi=0.5 and $Re=Re_1$

results is due to the utilization of generalized flow model to present fluid transport through porous medium in the work by Marafie and Vafai [29]. As expected, at lower values of the Biot number, a larger temperature difference is seen between the fluid and solid phases, due to a weak internal heat exchange between the fluid and solid. Next, the analytical temperature distribution for the case with an adiabatic upper wall is compared with the numerical results in Figs. 4 and 5. The comparisons indicate a very good agreement for the temperature profiles between the numerical and the analytical one equation model at different inclination angles (0 deg, 2 deg) and different longitudinal locations ($X=1,4$). The wall temperature distribution is also investigated to obtain a better understanding of the optimization and production of an isothermal surface. The analytical wall temperature distributions are compared with numerical simulations at different inclination angles in Fig. 6. Once again the analytical and numerical results are in excellent agreement.

To investigate the heat transfer aspects on production of an isothermal surface, the variations in the pertinent controlling parameters, such as inclination angle (α), Bi, and κ are investigated to illustrate their influence on the fluid and solid temperature distributions (Figs. 7 and 8). As can be seen in Figs. 7 and 8 an increase in the inclination angle, over a wide range, results in a more uniform solid temperature profile. The fluid temperature profile follows the same trend, except for low values of Bi and κ (Fig. 8(*b*)). For low values of κ, the heat exchange between the fluid and solid dominates over the conduction process as can be surmised from Eqs. (10) and (11). As such, an increase in the incli-

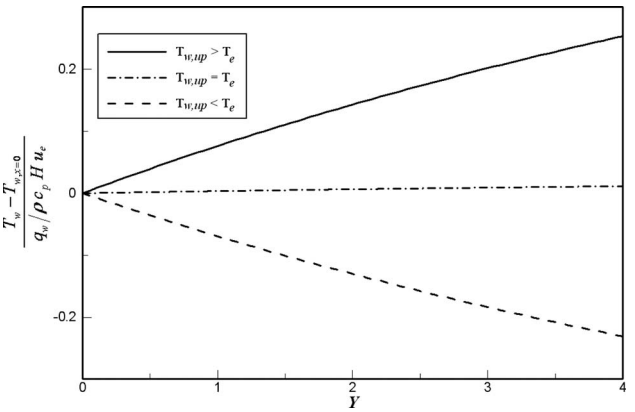

Fig. 11 Effect of the upper wall temperature (Case II) on the isothermal surface production for Bi=10, $\kappa=0.01$, and $\alpha=0$

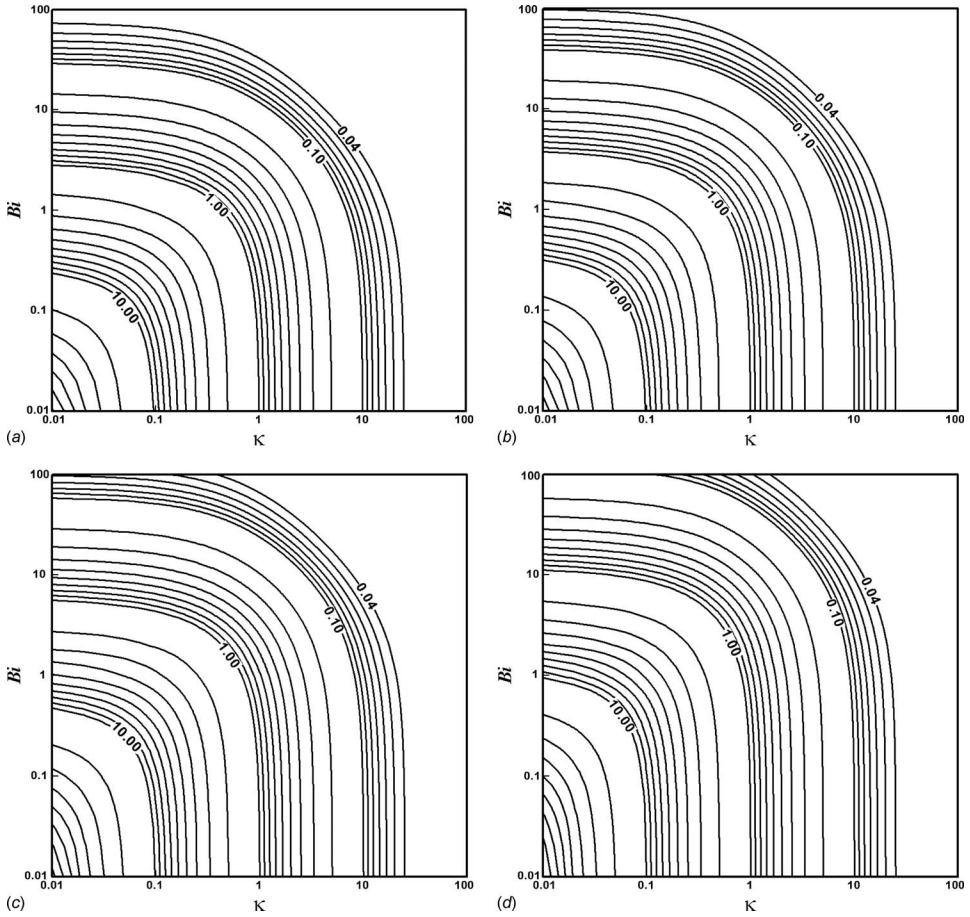

Fig. 12 Error maps on the validity of local thermal equilibrium model in the variable area channel heat exchanger: (*a*) ψ=1, (*b*) ψ=0.75, (*c*) ψ=0.5, and (*d*) ψ=0.25

nation angle at low Bi results in more deviation for the fluid phase temperature from that of the solid and the wall. However, at higher values of Bi, the inclination angle can be utilized as a valuable and effective parameter to control the wall temperature uniformity, as illustrated later in this work. The effect of Bi and κ on the temperature field at downstream locations is also investigated for nonzero inclination angles, which show trends that are similar to those shown in Figs. 7 and 8. Downstream locations are accompanied with a decrease in the channel thickness resulting in a larger convective term and heat exchange between the fluid and solid phases.

To illustrate characterization and production of an isothermal surface, the effects of the controlling parameters, $\psi(\alpha,x)$, Bi, and κ, on the wall temperature are shown in Figs. 9 and 10. Figures 9 and 10 indicate that for high effective thermal conductivity ratios (κ), changing the inclination angle does not considerably change the temperature uniformity, due to the dominating effect of the conduction over that of the fluid/solid heat exchange. However, at low thermal conductivity ratios (κ), increasing the inclination angle can modify the temperature profile. The effect of flow rate on the wall temperature distribution is also investigated in Fig. 9. The parameter Re_1 in this figure indicates a reference Reynolds number for investigating the flow rate effect. The results show that increasing the flow rate yields a more uniform temperature at the wall. For higher flow rates, the effects of inclination angle are quite substantial at high values of Bi and low values of κ. The effect of high flow rate in the cases with high value of κ can be very low due to the dominating effect of conduction in high κ.

A decrease in the effective thermal conductivity ratio can result in larger temperature values due to a decrease in heat exchange between the wall and the working fluid (Figs. 9 and 10). Also, at lower values of κ, a decrease in Biot number (at the same flow rate) results in larger wall temperature values due to a decrease in internal heat transport between the fluid and solid phases. Furthermore, for very low κ and Bi, an increase in the inclination angle can result in a slightly nonuniformity in the wall temperature (Fig. 10). For the second type of heat exchanger (Case II), the upper wall temperature also plays a role in isothermal surface production, while the effect of other parameters that have been studied earlier remains the same. Figure 11 indicates that an upper wall temperature smaller or larger than the entry temperature (T_e) can result in a more nonuniform temperature distribution, since as expected the upper wall is being employed to cool or heat the working fluid along the longitudinal direction.

To investigate the validity of local thermal equilibrium model, contour error maps are introduced based on the Nusselt number analytical expressions. As seen in Fig. 12, the error in utilizing the one equation model decreases for larger values of either the Biot number (Bi) or the effective thermal conductivity ratio (κ) or both. For larger interfacial fluid-solid heat exchange, the fluid and solid temperature distributions approach that of the one equation model indicating a small error when utilizing the one equation model. As Fig. 12 indicates, a decrease in the upper wall shape factor (ψ) reduces the validity of one equation model for a given Biot number.

4 Conclusions

Key issues in a number of thermal management devices, which may be required in biological, electronic, optical, laser, manufac-

turing, and solidification applications, are the production and regulation of an isothermal surface when it is subject to an imposed heat flux. In this work, analytical correlations are established to design a compact device capable of producing an isothermal surface. The analytical results were obtained considering negligible natural convection and radiation, hydraulically and thermally fully developed flow through the device, and homogenous and isotropic porous material. Exact solutions are presented for the fluid phase, porous substrate and surface temperature fields incorporating the local thermal nonequilibrium conditions. Nusselt number correlations are also established analytically for a generic variable cross sectional heat exchanger. These analytical results can be used as design formulas to prescribe the precise form of the setup for production of an isothermal surface. The investigation of the effect of the pertinent physical parameters indicate that the surface temperature uniformity can be regulated utilizing the inclination angle, especially for high flow rates and Biot numbers, due to larger heat exchange between the fluid and solid phases. It is established that an increase in the inclination angle results in a more uniform fluid and solid phase temperature distribution within the channel. At high effective fluid to solid thermal conductivity ratios, the fluid conduction dominates the effects of convection and the inclination angle. Utilization of the variable cross sectional area channel is also quite effective in augmenting the local Nusselt number and convective heat transfer coefficient on a surface subject to a constant heat flux. Both an insulated and a constant temperature sloped surface are considered in the analysis. It is found that utilization of local thermal equilibrium model leads to accurate results only at very high Biot numbers or at high effective fluid to solid thermal conductivities ratio. Furthermore, it is found that a decrease in the value of the upper wall shape factor (ψ) reduces the validity of the local thermal equilibrium model under the same physical conditions.

Acknowledgment

The grant from Ohio Supercomputer Center (OSC) is acknowledged and appreciated.

Nomenclature

a_{sf} = interfacial area per unit volume of porous media (m^{-1})
Bi = Biot number, $h_{sf}a_{sf}H^2/k_{s,\mathrm{eff}}$
c_p = specific heat of the working fluid ($J\,kg^{-1}\,K^{-1}$)
D_h = hydraulic diameter of the channel, $2H$(m)
E = error incurred in using the thermal equilibrium model $(\mathrm{Nu}_{w,\mathrm{equil}}-\mathrm{Nu}_{w,\mathrm{nonequil}})/\mathrm{Nu}_{w,\mathrm{nonequil}}$
h_{sf} = interstitial heat transfer coefficient ($W\,m^{-2}\,K^{-1}$)
$h_{w,\mathrm{nonequil}}$ = wall heat transfer coefficient for the thermal nonequilibrium model, $q_w/(T_w-T_{f,b})$ ($W\,m^{-2}\,K^{-1}$)
H = thickness of the channel entrance (m)
$k_{f,\mathrm{eff}}$ = effective thermal conductivity of the fluid phase ($W\,m^{-1}\,K^{-1}$)
$k_{s,\mathrm{eff}}$ = effective thermal conductivity of the solid phase ($W\,m^{-1}\,K^{-1}$)
$\mathrm{Nu}_{w,\mathrm{equil}}$ = Nusselt number of the wall subject to constant heat flux for the thermal equilibrium model
$\mathrm{Nu}_{w,\mathrm{nonequil}}$ = Nusselt number of the wall subject to constant heat flux for the thermal nonequilibrium model
q_w = heat flux at the wall ($W\,m^{-2}$)
Re = Reynolds number
T = temperature (K)
T_e = fluid temperature at the channel entrance (K)
$T_{f,b}$ = fluid bulk temperature (K)
T_w = temperature of the wall subjected to the constant heat flux (K)
$T_{w,\mathrm{up}}$ = temperature of the upper wall of the channel (K)
u = velocity ($m\,s^{-1}$)
u_e = velocity at the channel entrance ($m\,s^{-1}$)
$\bar{u}$ = nondimensional velocity, $\langle u\rangle/u_eH/(H-x\tan\alpha)$
x = longitudinal coordinate (m)
X = nondimensional longitudinal coordinate, x/H
y = transverse coordinate (m)
Y = nondimensional transverse coordinate, $y/H-x\tan\alpha$

Greek Symbols

α = inclination angle
κ = ratio of the effective fluid conductivity to that of the solid, $k_{f,\mathrm{eff}}/k_{s,\mathrm{eff}}$
θ = nondimensional temperature
$\theta_{f,b}$ = nondimensional fluid bulk temperature
$\theta_{w,\mathrm{up}}$ = nondimensional upper wall temperature, $k_{s,\mathrm{eff}}(T_{w,\mathrm{up}}-T_w)/[Hq_w\sqrt{\psi}+k_{s,\mathrm{eff}}(1+\kappa)(T_{w,\mathrm{up}}-T_w)]$
$\Delta\theta$ = nondimensional temperature difference between the solid and fluid phases
ρ = fluid density ($kg\,m^{-3}$)
λ = parameter, $\sqrt{\mathrm{Bi}\psi(1+\kappa)/\kappa}$
ψ = upper wall shape factor, $(H-x\tan\alpha)^2/H^2$

Subscripts/Superscripts

b = bulk
eff = effective property
f = fluid phase
s = solid phase
w = wall subjected to the constant heat flux
w,up = upper wall of the channel

Symbol

$\langle\rangle$ = "local volume average" of a quantity

References

[1] Zhu, N., and Vafai, K., 1998, "Analytical Modeling of the Startup Characteristics of Asymmetrical Flat-Plate and Disk-Shaped Heat Pipes," Int. J. Heat Mass Transfer, **41**, pp. 2619–2637.
[2] Wang, Y., and Vafai, K., 2000, "An Experimental Investigation of the Thermal Performance of an Asymmetrical Flat Plate Heat Pipe," Int. J. Heat Mass Transfer, **43**, pp. 2657–2668.
[3] Jiang, P. X., Fan, M. H., Si, G. S., and Ren, Z. P., 2001, "Thermal-Hydraulic Performance of Small Scale Micro-Channel and Porous-Media Heat-Exchangers," Int. J. Heat Mass Transfer, **44**(5), pp. 1039–1051.
[4] Lee, D. Y., and Vafai, K., 1999, "Comparative Analysis of Jet Impingement and Microchannel Cooling for High Heat Flux Applications," Int. J. Heat Mass Transfer, **42**, pp. 1555–1568.
[5] Vafai, K., and Zhu, L., 1999, "Analysis of a Two Layered Microchannel Heat Sink Concept in Electronic Cooling," Int. J. Heat Mass Transfer, **42**, pp. 2287–2297.
[6] Khaled, A. R., and Vafai, K., 2003, "The Role of Porous Media in Modeling Flow and Heat Transfer in Biological Tissues," Int. J. Heat Mass Transfer, **46**, pp. 4989–5003.
[7] Mahjoob, S., Vafai, K., and Beer, N. R., 2008, "Rapid Microfluidic Thermal Cycler for Polymerase Chain Reaction Nucleic Acid Amplification," Int. J. Heat Mass Transfer, **51**(9-10), pp. 2109–2122.
[8] Khanafer, K., and Vafai, K., 2001, "Isothermal Surface Production and Regulation for High Heat Flux Applications Utilizing Porous Inserts," Int. J. Heat Mass Transfer, **44**, pp. 2933–2947.
[9] Hetsroni, G., Mosyak, A., Segal, Z., and Ziskind, G., 2002, "A Uniform Temperature Heat Sink for Cooling of Electronic Devices," Int. J. Heat Mass Transfer, **45**(16), pp. 3275–3286.
[10] Erickson, D., and Li, D., 2004, "Integrated Microfluidic Devices," Anal. Chim. Acta, **507**(1), pp. 11–26.
[11] Mahjoob, S., and Vafai, K., 2008, "Analytical Characterization of Heat Transport Through Biological Media Incorporating Hyperthermia Treatment," Int. J. Heat Mass Transfer, in press.
[12] Kupchella, K., Clemons, C. B., Golovaty, D., and Young, G. W., 2006, "An Asymptotic Analysis for Directional Solidification of a Diffusion-Dominated Binary System," J. Cryst. Growth, **292**(1), pp. 111–124.
[13] Brown, R. A., 1988, "Theory of Transport Processes in Single Crystal Growth from the Melt," AIChE J., **34**(6), pp. 881–911.

[14] McLean, M., 1983, *Directionally Solidified Materials for High Temperature Service*, The Metals Society, London.
[15] Kermanpur, A., Rappaz, M., Varahram, N., and Davami, P., 2000, "Thermal and Grain-Structure Simulation in a Land-Based Turbine Blade Directionally Solidified With the Liquid Metal Cooling Process," Metall. Mater. Trans. B, **31**(6), pp. 1293–1304.
[16] Wang, Y., Amiri, A., and Vafai, K., 1999, "An Experimental Investigation of the Melting Process in a Rectangular Enclosure," Int. J. Heat Mass Transfer, **42**, pp. 3659–3672.
[17] Desai, C. P., and Vafai, K., 1993, "A Unified Critical Re-examination of the Melting Process in a Cavity," ASME J. Heat Transfer, **115**, pp. 1072–1075.
[18] Wilson, R. N., 1999, *Reflecting Telescope Optics II: Manufacture, Testing, Alignment, Modern Techniques*, Springer, New York.
[19] Barnes, W. P., 1966, "Some Effects of Aerospace Thermal Environments on High-Acuity Optical Systems," Appl. Opt., **5**(5), pp. 701–711.
[20] Sozen, M., and Vafai, K., 1990, "Analysis of the Non-Thermal Equilibrium Condensing Flow of a Gas Through a Packed Bed," Int. J. Heat Mass Transfer, **33**, pp. 1247–1261.
[21] Vafai, K., and Sozen, M., 1990, "Analysis of Energy and Momentum Transport for Fluid Flow Through a Porous Bed," ASME J. Heat Transfer, **112**, pp. 690–699.
[22] Sozen, M., and Vafai, K., 1993, "Longitudinal Heat Dispersion in Packed Beds with Real Gas Flow," J. Thermophys. Heat Transfer, **7**, pp. 153–157.
[23] Sozen, M., and Vafai, K., 1991, "Analysis of Oscillating Compressible Flow Through a Packed Bed," Int. J. Heat Fluid Flow, **12**, pp. 130–136.
[24] Vafai, K., and Sozen, M., 1990, "An Investigation of a Latent Heat Storage Packed Bed and Condensing Flow Through it," ASME J. Heat Transfer, **112**, pp. 1014–1022.
[25] Amiri, A., and Vafai, K., 1994, "Analysis of Dispersion Effects and Non-Thermal Equilibrium, Non-Darcian, Variable Porosity Incompressible Flow Through Porous Medium," Int. J. Heat Mass Transfer, **37**, pp. 939–954.
[26] Amiri, A., Vafai, K., and Kuzay, T. M., 1995, "Effect of Boundary Conditions on Non-Darcian Heat Transfer Through Porous Media and Experimental Comparisons," Numer. Heat Transfer, Part A, **27**, pp. 651–664.
[27] Alazmi, B., and Vafai, K., 2002, "Constant Wall Heat Flux Boundary Conditions in Porous Media Under Local Thermal Non-Equilibrium Conditions," Int. J. Heat Mass Transfer, **45**, pp. 3071–3087.
[28] Lee, D. Y., and Vafai, K., 1999, "Analytical Characterization and Conceptual Assessment of Solid and Fluid Temperature Differentials in Porous Media," Int. J. Heat Mass Transfer, **42**, pp. 423–435.
[29] Marafie, A., and Vafai, K., 2001, "Analysis of Non-Darcian Effects on Temperature Differentials in Porous Media," Int. J. Heat Mass Transfer, **44**, pp. 4401–4411.
[30] Poulikakos, D., and Renken, K., 1987, "Forced Convection in a Channel Filled With Porous Medium, Including the Effects of Flow Inertia, Variable Porosity, and Brinkman Friction," ASME J. Heat Transfer, **109**(4), pp. 880–888.
[31] Vafai, K., and Kim, S., 1989, "Forced Convection in a Channel Filled With Porous Medium—An Exact Solution," ASME J. Heat Transfer, **111**, pp. 1103–1106.
[32] Hunt, M. L., and Tien, C. L., 1988, "Effects of Thermal Dispersion on Forced Convection in Fibrous Media," Int. J. Heat Mass Transfer, **31**(2), pp. 301–309.
[33] Mahjoob, S., and Vafai, K., 2008, "A Synthesis of Fluid and Thermal Transport Models for Metal Foam Heat Exchangers," Int. J. Heat Mass Transfer, **51**(15-16), pp. 3701–3711.
[34] Calmidi, V. V., and Mahajan, R. L., 2000, "Forced Convection in High Porosity Metal Foams," ASME J. Heat Transfer, **122**, pp. 557–565.
[35] Phanikumar, M. S., and Mahajan, R. L., 2002, "Non-Darcy Natural Convection in High Porosity Metal Foams," Int. J. Heat Mass Transfer, **45**, pp. 3781–3793.
[36] Combarnous, M. A., and Bories, S. A., 1975, "Hydrothermal Convection in Saturated Porous Media," Adv. Hydrosci., **10**, pp. 231–307.
[37] Cheng, P., 1978, "Heat Transfer in Geothermal Systems," Adv. Heat Transfer, **14**, pp. 1–105.
[38] Tien, C. L., and Vafai, K., 1989, "Convective and Radiative Heat Transfer in Porous Media," Adv. Appl. Mech., **27**, pp. 225–282.
[39] Hadim, H., and Vafai, K., 2000, "Overview of Current Computational Studies of Heat Transfer in Porous Media and their Applications—Forced Convection and Multiphase Transport," *Advances in Numerical Heat Transfer*, Taylor & Francis, New York, pp. 291–330.
[40] Vafai, K., and Hadim, H., 2000, "Overview of Current Computational Studies of Heat Transfer in Porous Media and their Applications—Natural Convection and Mixed Convection," *Advances in Numerical Heat Transfer*, Taylor & Francis, New York, pp. 331–371.
[41] 2006, FLUENT 6.3 User's Guide, Lebanon US.
[42] Patankar, S. V., 1980, *Numerical Heat Transfer and Fluid Flow*, McGraw-Hill, New York.